Single Channel Analysis of Conductance and Rectification in Cation-selective, Mutant Glycine Receptor Channels

Andrew J. Moorhouse,[1] Angelo Keramidas,[1] Andrey Zaykin,[1] Peter R. Schofield,[2] and Peter H. Barry[1]

[1]Department of Physiology and Pharmacology, University of New South Wales, Sydney 2052, Australia
[2]The Garvan Institute of Medical Research, Darlinghurst, Sydney 2010, Australia

ABSTRACT Members of the ligand-gated ion channel superfamily mediate fast synaptic transmission in the nervous system. In this study, we investigate the molecular determinants and mechanisms of ion permeation and ion charge selectivity in this family of channels by characterizing the single channel conductance and rectification of α1 homomeric human glycine receptor channels (GlyRs) containing pore mutations that impart cation selectivity. The A-1'E mutant GlyR and the selectivity double mutant ([SDM], A-1'E, P-2'Δ) GlyR, had mean inward chord conductances (at −60 mV) of 7 pS and mean outward conductances of 11 and 12 pS (60 mV), respectively. This indicates that the mutations have not simply reduced anion permeability, but have replaced the previous anion conductance with a cation one. An additional mutation to neutralize the ring of positive charge at the extracellular mouth of the channel (SDM+R19'A GlyR) made the conductance–voltage relationship linear (14 pS at both 60 and −60 mV). When this external charged ring was made negative (SDM+R19'E GlyR), the inward conductance was further increased (to 22 pS) and now became sensitive to external divalent cations (being 32 pS in their absence). The effects of the mutations to the external ring of charge on conductance and rectification could be fit to a model where only the main external energy barrier height for permeation was changed. Mean outward conductances in the SDM+R19'A and SDM+R19'E GlyRs were increased when internal divalent cations were absent, consistent with the intracellular end of the pore being flanked by fixed negative charges. This supports our hypothesis that the ion charge selectivity mutations have inverted the electrostatic profile of the pore by introducing a negatively charged ring at the putative selectivity filter. These results also further confirm the role of external pore vestibule electrostatics in determining the conductance and rectification properties of the ligand-gated ion channels.

KEY WORDS: ligand-gated ion channels • rings of charge • ion permeation • ion selectivity • M2 domain

INTRODUCTION

The ligand-gated ion channels (LGICs)* mediate fast synaptic transmission in the central and peripheral nervous system. In most physiological conditions, the cation-selective nicotinic acetylcholine receptor channels (nAChRs) and the serotonin type 3 receptor channels (5-HT_3Rs) mediate depolarizing, excitatory responses, whereas the anion selective γ-aminobutyric acid receptor channels ($GABA_A$Rs, $GABA_C$Rs) and glycine receptor channels (GlyRs) mediate hyperpolarizing, inhibitory responses. All the members of this channel superfamily are pentameric proteins, with the M2 domain of each subunit contributing to the channel pore. The M2 domain contains charged amino acids at their extracellular, intracellular, and cytoplasmic borders (Fig. 1). The cytoplasmic ring of charge is negative in all the LGICs, whereas the intracellular and extracellular rings are negative in the cation-selective nAChRs and positive in the anion-selective GlyRs and GABARs (for reviews see Changeux, 1993; Unwin, 1993; Karlin and Akabas, 1995). The role of these charged rings in ion permeation in the nAChR has been extensively studied. Monovalent cation conductance is decreased as the charge on these rings is decreased, with the greatest effects occurring for mutations to the intermediate ring (Imoto et al., 1988). Furthermore, in the nAChR, the extracellular and intracellular rings of charge provide a structural basis for inhibition of monovalent cation conductance by extracellular and intracellular divalent cations, respectively (Imoto et al., 1988; Kienker et al., 1994; Forster and Bertrand, 1995). Much less detail is known about the role of charged rings in permeation in other members of the LGIC family, although mutations which neutralize the extracellular ring of positive charge in GlyRs reduce inward anion conductance (Langosch et al., 1994; Rajendra et al., 1995).

Address correspondence to Peter H. Barry, Department of Physiology and Pharmacology, University of New South Wales, Sydney 2052, Australia. Tel.: (61) 2-9385-1101; Fax: 61-2-9385-1099; E-mail: p.barry@unsw.edu.au

*Abbreviations used in this paper: 5-HT_3Rs, serotonin type 3 receptor-channels; $GABA_A$R, γ-aminobutyric acid receptor channel; GlyR, glycine receptor-channel; LGIC, ligand-gated ion channel; nAChR, nicotinic acetylcholine receptor channel; R.I., rectification index; SDM, selectivity double mutant; STM, selectivity triple mutant; 293 cell, human embryonic kidney 293 cell.

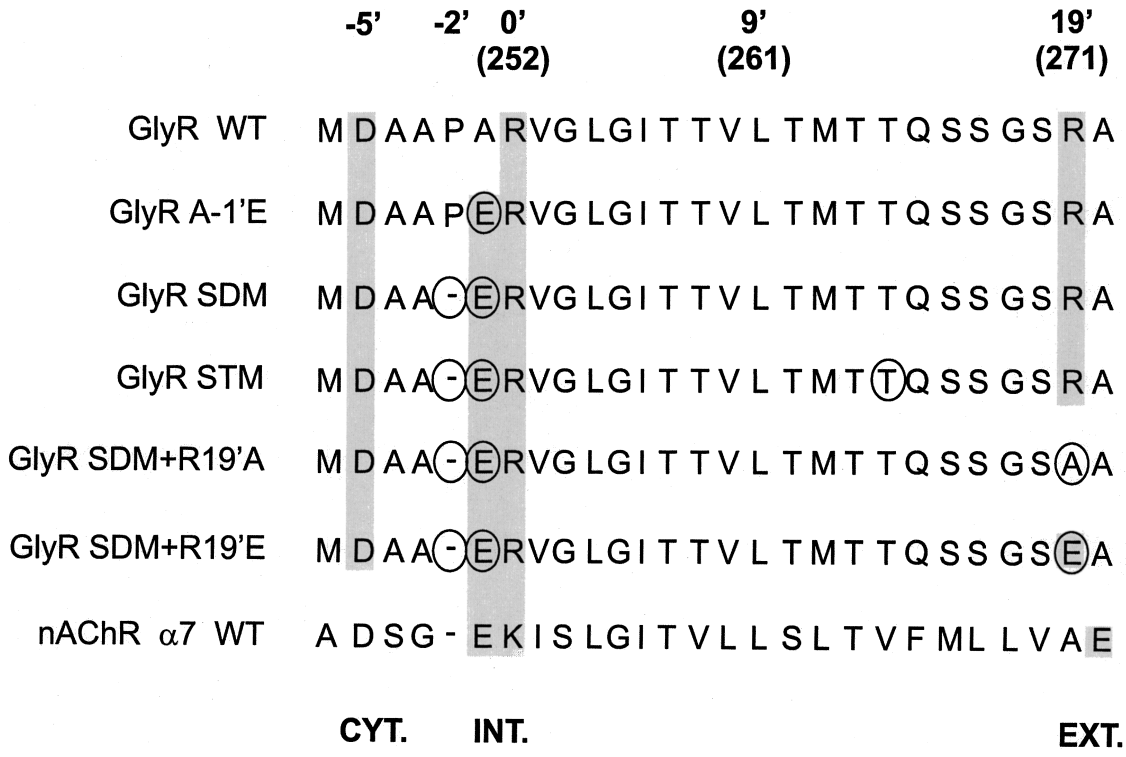

FIGURE 1. Amino acids in the M2 domains of the α1 WT (Grenningloh et al., 1987) and the cation-selective mutant GlyRs. For comparison, the amino acids in the M2 domain of the α7 subunit of the nAChR (Couturier et al., 1990) are also shown. The individual mutations introduced into the α1 WT GlyR, which confer cation selectivity, are circled. For the GlyRs, filled boxes illustrate basic or acidic residues in the cytoplasmic (CYT), intermediate (INT), and extracellular (EXT) rings of charged amino acids (compare Imoto et al., 1988). The residue numbering system, indicated with a'(prime), is taken relative to the internal charged arginine (R0') with the conventional GlyR primary sequence number shown in parenthesis.

Mutations to the nAChR which neutralize or invert the charge on the extracellular ring of the nAChR have not, however, been reported to alter ion charge selectivity. Instead, the molecular basis for cation or anion selectivity within the LGIC family is mediated by other differences in the amino acid sequence of the pore forming M2 domains. Our accompanying paper (Keramidas et al., 2002, this issue) clearly demonstrated the importance of the region around the intermediate ring of charge in determining ion charge selectivity. This region is thought to be where the pore is most constricted (Lester, 1992; Imoto, 1993; Wilson and Karlin, 1998). A single point mutation within this region (A-1'E GlyR) was sufficient to convert the channel to being cation selective, whereas the addition of P-2'Δ to this mutant (selectivity double mutant [SDM] or A-1'E, P-2'Δ GlyR) produced a more cation-selective channel which also allowed the permeation of divalent cations. Additional changes to the charge at the extracellular ring, neutralization (SDM+R19'A GlyR) or inversion (SDM+R19'E GlyR) of the extracellular ring of charged arginine residues, accentuated Ca^{2+} permeability, but did not further increase relative monovalent cation to anion selectivity. This constricted region also plays an important role in determining ion charge selectivity in the α7 homomeric nACh (Galzi et al., 1992; Corringer et al., 1999), although the single inverse (E-1'A) mutation did not convert the nAChR into being anion-selective. The E-1'A mutation had to be coupled with the insertion of a proline between −1' and −4', and an additional mutation at the 13' or 9' position was necessary to observe robust currents. It has been inferred that ion-charge selectivity is achieved by interactions between permeating ions and the peptide backbone, rather than with charged amino acid side chains (Corringer et al., 1999). This has led to suggestions that selectivity conversion involves some quite marked structural rearrangement of the channel pore, especially around this constricted region, and is not simply due to the addition or removal of charged amino acid side chains (Corringer et al., 1999; Gunthorpe and Lummis, 2001). We (Barry and Fatima-Shad, 1995; Keramidas et al., 2000, 2002, this issue) and others (Imoto, 1993) have postulated that selectivity conversion primarily arises due to a change in the amino acid side chains which may contribute to the intrinsic electrical potential of the pore. That is, the lysine at 0' becomes exposed and electrostatically dominant in the anion-

selective mutated nAChRs, whereas, in the cation selective GlyR mutants, the arginine at 0' becomes shielded or electrostatically dominated by the introduced E-1'. The presence of a negatively charged side chain at the intracellular end of the pore in the cation-selective mutant GlyRs should facilitate cation conductance. Furthermore, it may create a site(s) for mediating an inhibition of monovalent cation conductance by divalent cations, as occurs in nAChRs (Imoto et al., 1988; Forster and Bertrand, 1995) and other cation channels (e.g., Heinemann et al., 1992; Root and MacKinnon, 1993; Yang et al., 1993).

The aim of this study was to gain further insight into permeation in LGICs by investigating the single channel conductance and rectification properties of these cation selective mutant GlyRs. Initially, we wished to quantify the conductances to assess whether the mutants simply abolished chloride permeability or had replaced the previous wild-type (WT) GlyR chloride conductance with a significant cation conductance. Primarily, however, we wished to investigate whether these mutant GlyR pores were flanked by rings of charged amino acids and, if so, investigate their influence on conductance and rectification. Our hypothesis of the structural mechanisms underlying conversion of ion-charge selectivity in the cation-selective mutant GlyRs predicts a ring of negative charge at the intracellular end of the pore. Finally, we explored what effects these mutations also had on the sensitivity to glycine and on the current activation and decay kinetics.

MATERIALS AND METHODS

Transient Expression of Recombinant α1 Subunit GlyRs in 293 Cells

The molecular biological techniques are identical to those described previously (Keramidas et al., 2000). Briefly, complementary DNA (cDNA) encoding the α1 subunit of the human GlyR was subcloned into the pCIS expression vector and used to transfect human embryonic kidney 293 (293) cells using the calcium phosphate precipitate method of Chen and Okayama (1987). The 293 cells were cotransfected with the expression marker, CD4 surface antigen, and used for recordings between 1–3 d following transfection. A range of α1 GlyR mutant channels were investigated in this study, all of which had point mutations in, or flanking, the M2 transmembrane domain, as illustrated in Fig. 1. These were: (a) the A-1'E (A251E) mutant, (b) SDM with A-1'E and P-2'Δ (P250Δ), (c) the SDM+R19'A mutation with R19'A (R271A), P-2'Δ, and A-1'E, and (d) the SDM+R19'E mutation with R19'E (R271E), P-2'Δ, and A-1'E.

Solutions

All solute concentrations given below are in mM. The standard intracellular (pipette) solution consisted of: 145 NaCl, 2 $CaCl_2$, 2 $MgCl_2$, 10 HEPES, 5 EGTA adjusted to pH 7.3 with NaOH. The standard extracellular (bath) solution consisted of: 145 NaCl, 2 $CaCl_2$, 2 $MgCl_2$, 10 HEPES, 10 glucose, adjusted to pH 7.4 with NaOH. In some experiments Ca^{2+} and Mg^{2+} were omitted from the bath and pipette solutions to give nominally divalent free solutions. Liquid junction potentials arising from pipette and bath solutions were calculated using the Windows version of the software package *JPCalc* (Barry, 1994). Experiments were performed at a room temperature of 21 ± 2°C.

For the single channel recordings, and for the macroscopic current concentration-response curve data, glycine was added to the bath using a slow, gravity-fed bath perfusion system. For the whole-cell current recordings, glycine was applied directly to the cell under study using a gravity-fed parallel array of polythene microperfusion tubes mounted on an electromechanical micromanipulator (open pipette response times ~15–20 ms).

Electrophysiology

All patch pipettes were pulled using a two-stage electrode puller (Sutter Instruments Co.) and fire-polished. Borosilicate haematocrit tubes (Vitrex-1601), with resistances, when filled with intracellular solution and measured in the bath solution, between 1.4 and 2.7 MΩ, were used for whole-cell recordings. For these recordings, series resistances ranged between 2 and 11 MΩ and were compensated for between 75–80%. Whole-cell membrane currents were recorded using an Axopatch-1D amplifier, digitized using a Digidata 1200 A/D board and recorded using *pCLAMP 8* software (all from Axon Instruments, Inc.) on a Pentium 166 MHz computer. Currents were filtered with the 4-pole Bessel filter (provided on the amplifier) at a −3 dB setting of 500 Hz and acquired at a sampling frequency of 1 kHz.

For single channel experiments, patch pipettes were made using thick-walled borosilicate glass capillaries (GC150F-15; Clark Electromedical Instruments). These were generally coated with Sylgard (Dow Corning) and fire-polished before use to give final resistances of 8–15 MΩ when filled with pipette solution. Single channel currents were recorded from excised outside-out membrane patches, typically held at membrane potentials between 60 and −60 mV, in response to the bath application of glycine. Currents were recorded with *pCLAMP 8* software and an Axopatch 200B amplifier (Axon Instruments, Inc.) and were digitized at 10 kHz directly onto the hard disk of a 166 MHz Pentium computer (via a Digidata 1200; Axon Instruments, Inc.) after filtering with the amplifier's 4-pole Bessel filter at a −3 dB setting of 2 kHz.

Data Analysis

Single channel current amplitudes were quantified by direct measurements using horizontal cursors placed on the estimated mean baseline and open current levels and by the mean of Gaussian distributions that were fitted to all-point amplitude histograms (bin sizes: 0.03–0.10 pA) using a least squares minimization procedure. All analysis used *pCLAMP 8* software (Axon Instruments, Inc.). Additional digital Gaussian filtering up to 700 Hz was applied to some records. In these situations, the conductance values obtained were confirmed by analyzing the same recordings, either unfiltered or filtered less. All-point histograms were constructed from selected sections of the recordings with transitions between baseline current and a clear single channel open current level. Conductances were calculated by dividing the current by the driving force ($V_m - V_{rev}$), with V_{rev} being approximated to zero for these NaCl solutions that are very close to symmetrical. In some patches a subconductance state was observed and the corresponding histogram was fit significantly better with the sum of three, rather than two, Gaussian distributions. As these subconductance states were rare and inconsistent, only the dominant conductance level has been further analyzed and reported here. The dominant conductance state was also typically the largest conductance level.

TABLE I

Activation and Desensitization Rates of WT and Mutant GlyR Whole-cell Currents

	WT (6)	A-1'E (7)	SDM (9)	SDM+R19'A (8)	SDM+R19'E (7)
Time to peak (ms)	51 ± 14	340 ± 35	860 ± 210	2190 ± 390	2400 ± 560
10–90% rise time (ms)	17 ± 8	160 ± 18	230 ± 170	890 ± 210	1140 ± 550
Fractional decay[a]	48 ± 5%	95 ± 2%	4 ± 1%	3 ± 1%	4 ± 2%
τ_{decay} (ms)	1860 ± 230	650 ± 80	flat	flat	flat

All data were obtained using whole cell currents recorded from 293 cells expressing the WT GlyR or the A-1'E, SDM, SDM+R19'A, or SDM+R19'E GlyR. All currents were recorded at −40 mV in response to an ~5 s application of a supramaximal glycine concentration. Data are means ± SEM, numbers in parentheses in the top row refer to the number of experiments (*n*), and the data are expressed to appropriate significant figures.

[a]Fractional decay refers to the extent of current decay from the peak current to the current recorded just before the end of the 5-s glycine application period. If the decay exceeded 5% of the peak amplitude then it was fitted with a single exponential function, giving the τ_{decay}. If this decay was <5% then τ_{decay} was denoted as "flat".

Off-line analysis of the rise and decay times for whole cell currents were conducted using *Clampfit* (*pCLAMP 8,* Axon Instruments). All currents were elicited at a holding potential of −40 mV in response to a 5 s application of a supramaximal glycine concentration. The time taken for the current amplitude to rise from 10 to 90% of its peak value, and the extent of current decay ("fractional decay") between the peak current and the current amplitude at the end of the glycine application period, was measured. If this fractional decay exceeded 5% of the peak value then a single exponential function was fit to the decay. Rise times and decay times were measured in each experiment and then averaged. All fits gave r^2 values above 0.90.

Concentration-response curves from individual experiments were fitted to the following Hill equation (Eq. 1) using a least squares minimization procedure (*SigmaPlot*; Jandell Scientific), and the EC_{50} and n_H values were then averaged for each mutant GlyR. For display, the data from each experiment were normalized with respect to the I_{max} value, averaged and then these mean data were fitted to Eq. 1.

$$I_{glycine} = I_{max}/(1 + EC_{50}{}^{nH}/[glycine]^{nH}) \quad (1)$$

where $I_{glycine}$ = the current activated by a given concentration of glycine, I_{max} = the maximal current activated by glycine, n_H = the Hill coefficient, and EC_{50} = the concentration of glycine which elicits a current that is 50% of I_{max}.

Statistical analysis used the paired or unpaired Student's *t* test, as appropriate. All data are expressed as mean ± SEM.

RESULTS

Macroscopic Current Kinetics and Concentration Response Curves

Before investigating the single channel properties of the mutant GlyRs, we first examined the macroscopic current kinetics and sensitivity to glycine. The rate of whole-cell current activation and decay, in response to relatively rapid application of a supramaximal glycine concentration, was examined in WT GlyRs and in the cation-selective GlyRs (SDM, SDM+R19'A, SDM+R19'E, and A-1'E [Fig. 2 A]), the results of which are summarized in Table I. All the cationic mutant GlyRs showed a slower rise in current, particularly the three SDM-based GlyRs, which took up to ~3 s to reach the peak amplitude, as opposed to <100 ms in the WT GlyRs. Even more striking is the apparent total lack of receptor desensitization in these SDM-based GlyRs. The current amplitude decayed by <5% when measured 2–3 s after the current peak, as opposed to an exponential decline to ~50% of the peak current in the WT GlyRs. In contrast, the A-1'E mutant GlyR displayed even greater fractional decay (by 95%) than the WT GlyR (48% fractional decay).

Concentration-response curves were generated for the SDM-based GlyRs using macroscopic current recordings in excised outside-out patches in response to slow bath application of glycine. As the whole-cell currents for the SDM-based set of mutant GlyRs showed virtually no desensitization during relatively rapid and maintained applications of glycine (above), slow bath perfusion should still provide an accurate measurement of peak current amplitude. This was not, however, an appropriate protocol for investigating the concentration-response properties of the rapidly desensitizing A-1'E mutant GlyR. The mean data is displayed in Fig. 2 B, which also includes, for comparison, concentration-response data obtained from a previous study on WT GlyRs using whole cell recordings and relatively rapid perfusion (Moorhouse et al., 1999; see also De Saint Jan et al., 2001). All mutant GlyRs showed a rightward shifted concentration-response curve compared with the WT GlyR. For the SDM and the SDM+R19'E GlyRs, the extent of this shift was comparable, with an ~20-fold increase in EC_{50} to 420 ± 80 μM (n = 3) and to 500 ± 70 μM (n = 3), respectively. The SDM+R19'A GlyR showed the largest rightward shift, with an ~400-fold increase in EC_{50} to 8,300 ± 800 μM (n = 3). The Hill coefficients for the three SDM-based GlyRs were reduced from 3.9 ± 0.9 in the WT (Moorhouse et al., 1999) to mean values of 1.90 ± 0.32 (SDM, n = 3), 1.44 ± 0.05 (SDM+R19'A, n = 3), and 1.70 ± 0.25 (SDM+R19'E, n = 3). The mean I_{max} values, which varied markedly from membrane patch to patch, ranged from ~50 to 300 pA across the set of GlyR mutants.

Conductance and Rectification in WT α1 GlyRs

Outside-out membrane patches excised from 293 cells expressing WT GlyRs displayed clear single channel

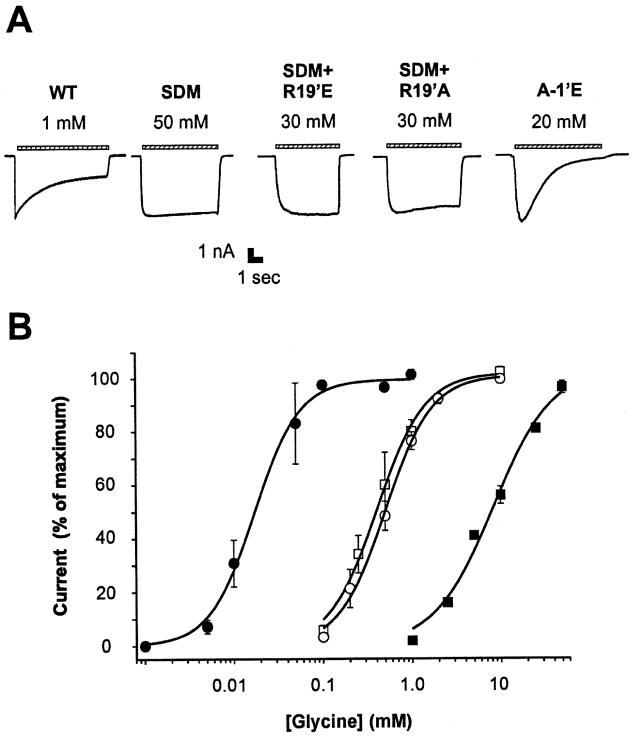

FIGURE 2. (A) Representative whole cell recordings for the WT GlyR and for the SDM, SDM+R19'A, SDM+R19'E, and A-1'E mutant GlyRs. In each case the current was elicited in response to a relatively rapid application of a supramaximal concentration of glycine, as indicated. All currents were recorded at a membrane voltage of −40 mV. Sample currents with comparable peak amplitudes were chosen to illustrate the differences in the time course of channel activation and desensitization between the GlyRs. (B) Mean concentration-response curves for the WT GlyR (filled circles, $n = 5$) and for the cation-selective mutant GlyRs, the SDM (open squares, $n = 3$), SDM+R19'A (filled squares, $n = 3$), and SDM+R19'E (open circles, $n = 3$). The WT GlyR data are reproduced from the whole cell recordings of Moorhouse et al. (1999), whereas, for the mutant GlyRs, data were obtained by recording the macroscopic current in excised outside-out patches in response to slow bath application of glycine. The mean data were fitted to Eq. 1 using a least squares minimization procedure with the resultant best fits shown by the curves. Fitting Eq. 1 to individual experiments gave a mean EC_{50} and n_H of, respectively, 23 ± 10 μM and 3.5 ± 0.9 for the WT GlyR, 420 ± 80 μM and 1.9 ± 0.3 for the SDM GlyR, 500 ± 70 μM and 1.7 ± 0.3 for the SDM+R19'E GlyR, and 8,300 ± 800 μM and 1.4 ± 0.1 for the SDM+R19'A GlyR.

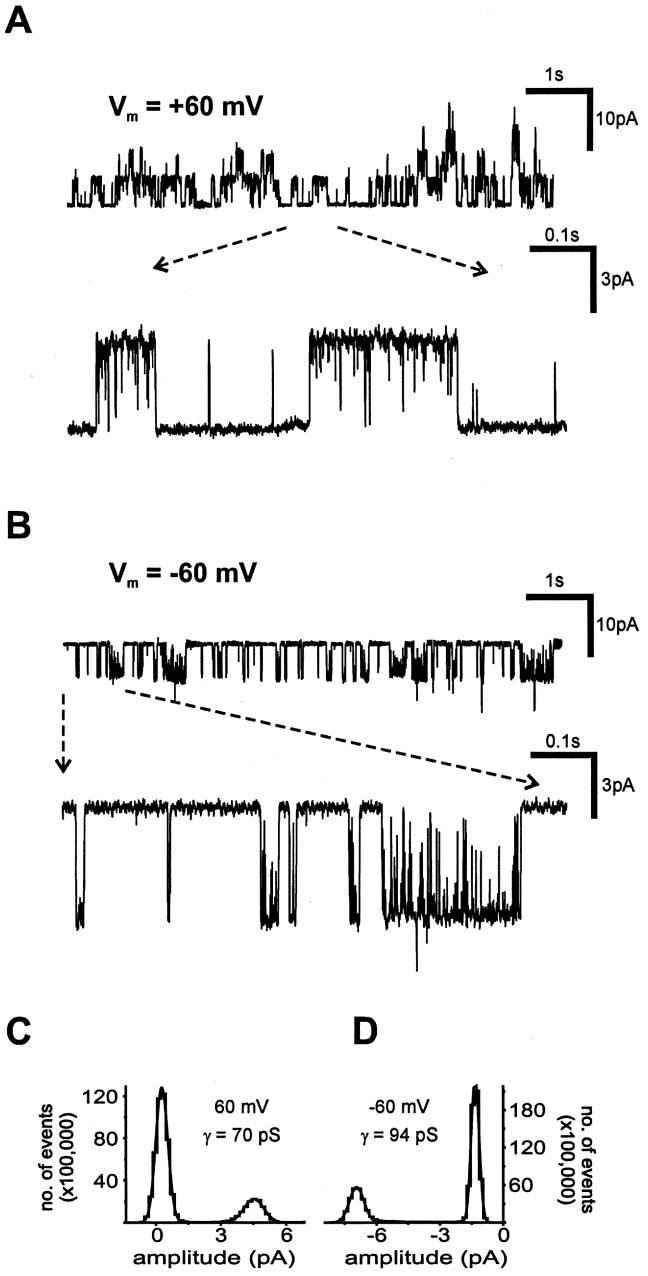

FIGURE 3. Representative single channel currents, and corresponding all-point amplitude histograms, from excised outside-out patches containing WT GlyRs. All currents were recorded in control 145 mM NaCl solutions with divalent cations present (see MATERIALS AND METHODS). (A) Outward currents recorded at a membrane potential of 60 mV. (B) Inward currents recorded at a membrane potential of −60 mV. In both A and B, the top panel shows ~8 s of continuous current recordings, whereas the lower panels show an ~0.8 s subset of this recording (the borders of which are indicated by the broken lines) expanded at higher resolution. Note the different scale bars for the top and bottom panels. C and D show the all-point amplitude histograms (bin widths 0.07–0.10 pA) compiled from longer segments (~2 min) from the same patches, at −60 mV (C) and 60 mV (D). The overlying curves are the sum of two Gaussian distributions fitted to the histograms using a least squares method, the means of which were used to calculate the conductance values for this patch, which are displayed above the histograms.

openings, at both −60 and 60 mV, in response to a low (~1 μM) concentration of glycine (Fig. 3). At both potentials, the GlyRs open in clear bursts, with the channel passing considerable current at each opening. Note the higher open probability at the positive potentials. The open channel current at each potential was derived from the mean of Gaussian fits to amplitude histograms, as illustrated in Figs. 3, C and D. At membrane potentials between −50 and −60 mV the dominant conductance level in six patches ranged from 74 to 100 pS (mean of 86.5 ± 4.1 pS; Table II), whereas for the same six patches

TABLE II

Summary of Conductance and Rectification Properties of WT and Cation-selective Mutant GlyRs

α1-GlyR	γ-60 mV	γ+60 mV	Rectification index[a]	
	pS	*pS*	*(I_{in} / I_{out})*	
WT	86.5 ± 4.1 (6)	62.2 ± 2.3 (6)	1.40 ± 0.08 (6)	inward
STM[b]	3.3 ± 0.4 (4)	11.1 ± 1.4 (3)	0.31 ± 0.65 (3)	outward
A-1'E	6.9 ± 0.2 (5)	11.1 ± 0.6 (4)	0.62 ± 0.01 (4)	outward
SDM	6.6 ± 0.3 (6)	12.4 ± 1.6 (5)	0.55 ± 0.05 (5)	outward
SDM+R19'A	13.5 ± 0.3 (13)	13.8 ± 0.6 (12)	1.00 ± 0.03 (12)	linear
SDM+R19'E	22.2 ± 0.7 (14)	16.4 ± 0.8 (13)	1.40 ± 0.09 (13)	inward

All data were obtained using excised outside-out patches from 293 cells expressing α1 WT or the various cation-selective mutant GlyRs, and also using the standard divalent cation containing ~145 mM symmetrical NaCl solutions (see MATERIALS AND METHODS). Data are mean ± SEM and numbers in parentheses indicate *n*.

[a]The R.I. was derived by dividing the conductance measured in each patch at −60 mV by that measured at 60 mV (γ−60 mV/γ+60 mV).

[b]For the STM GlyR, data are from Keramidas et al. (2000) and were obtained using noise analysis. For all other GlyRs, conductance values were obtained by direct measurements and from Gaussian fits to all-point histograms.

at membrane potentials between 50 and 60 mV, the main conductance level ranged from 54 to 68 pS (62.2 ± 2.3 pS; Table II). The extent of rectification in a single patch was quantified by dividing the conductance obtained at −50 or −60 mV by that obtained at the corresponding positive membrane potential. This rectification index (R.I.) ranged from 1.10 to 1.64 (1.40 ± 0.08; Table II), indicating that the WT GlyR shows inward rectification of the open channel current.

Conductance and Rectification in the Cation Selective Mutant GlyRs

Single channel conductance and rectification was investigated in the cation-selective GlyR mutants at membrane potentials of 60 and −60 mV. Typical examples of single channel current recordings are shown in Figs. 4 and 5. Clear single channel openings could be observed for all four of these cation-selective mutant GlyRs. For the A-1'E mutant GlyR (Figs. 4 B and 5, A and E), the amplitudes of the single channel openings were much reduced compared with WT and, furthermore, the inward currents were now smaller than the corresponding outward currents. For five patches held at a membrane potential of −50 or −60 mV, the mean single channel conductance was 6.9 ± 0.2 pS, whereas when four of the same patches were held at 60 mV, the mean outward conductance was 11.1 ± 0.6 pS. Thus, Na^+ conductances in this mutant are much lower compared with Cl^- conductances in the WT GlyR and the direction of rectification is reversed. In these same four A-1'E mutant GlyR patches the R.I. was 0.62 ± 0.01, thus demonstrating outward rectification.

For the SDM GlyR, the inward and outward currents and the extent of rectification were comparable to the A-1'E mutant GlyR (Figs. 4 C and 5, B and F). For six patches held at a membrane potential of −60 mV, the single channel conductance was 6.6 ± 0.3 pS, whereas when five of the same patches were held at 60 mV, the outward conductance was 12.4 ± 1.6 pS. In these patches, the R.I. was 0.55 ± 0.05. Thus, the A-1'E and SDM GlyRs have similar conductances and both display marked outward rectification.

We next investigated the role of the external ring of charge in permeation through the cation-selective mutant GlyRs, hypothesizing that the positively charged R19' residue would be electrostatically inappropriate for cationic currents as it would reduce the rapid flux of cations through the pore. Indeed, as shown in Figs. 4 and 5 and summarized in Table II, when we combined the SDM mutation with the neutralization of R19' (SDM+R19'A GlyR), inward currents were substantially increased. In 13 patches held at −50 or −60 mV the inward conductance was 13.5 ± 0.3 pS, whereas the corresponding mean outward conductance in 12 of these patches was 13.8 ± 0.6 pS. Thus, in addition to causing an increase in inward currents, the I-V relationship became linear (mean R.I. was 1.00 ± 0.03; $n = 12$). To further explore the role of charge at the 19' position, the SDM mutation was combined with the introduction of a negatively charged ring at the 19' position (SDM+R19'E GlyR). Inward conductance was further increased in these SDM+R19'E GlyRs, with only a relatively small increase in the outward conductance. The mean inward conductance, at −50 or −60 mV, was 22.2 ± 0.7 pS ($n = 14$), whereas the corresponding mean outward conductance was 16.4 ± 0.8 pS ($n = 13$). The increase seen in inward currents resulted in inward rectification, with the mean R.I. being 1.40 ± 0.09 ($n = 13$).

The effects of the R19' mutations can also be seen in Fig. 6 A, which plots the mean I-V relationship for the SDM+R19'A GlyR (open circles, $n = 5$) and the SDM+R19'E GlyR (filled circles, $n = 4$). The SDM+R19'A GlyR has a linear I-V curve, whereas the SDM+R19'E GlyR shows an increase in inward conductance, resulting in inward rectification.

Figure 4. Representative single channel currents from excised outside-out patches containing WT (A) or the cation-selective mutant GlyRs, A-1'E (B), SDM (C), SDM+R19'A (D), and SDM+R19'E (E). All currents were recorded in control 145 mM NaCl solutions with divalent cations present (see MATERIALS AND METHODS). For each receptor type, the panels show 20 s of current recordings, with the left panels being at a membrane potential of 60 mV and the right panels at −60 mV. In each panel, the current record is continuous,

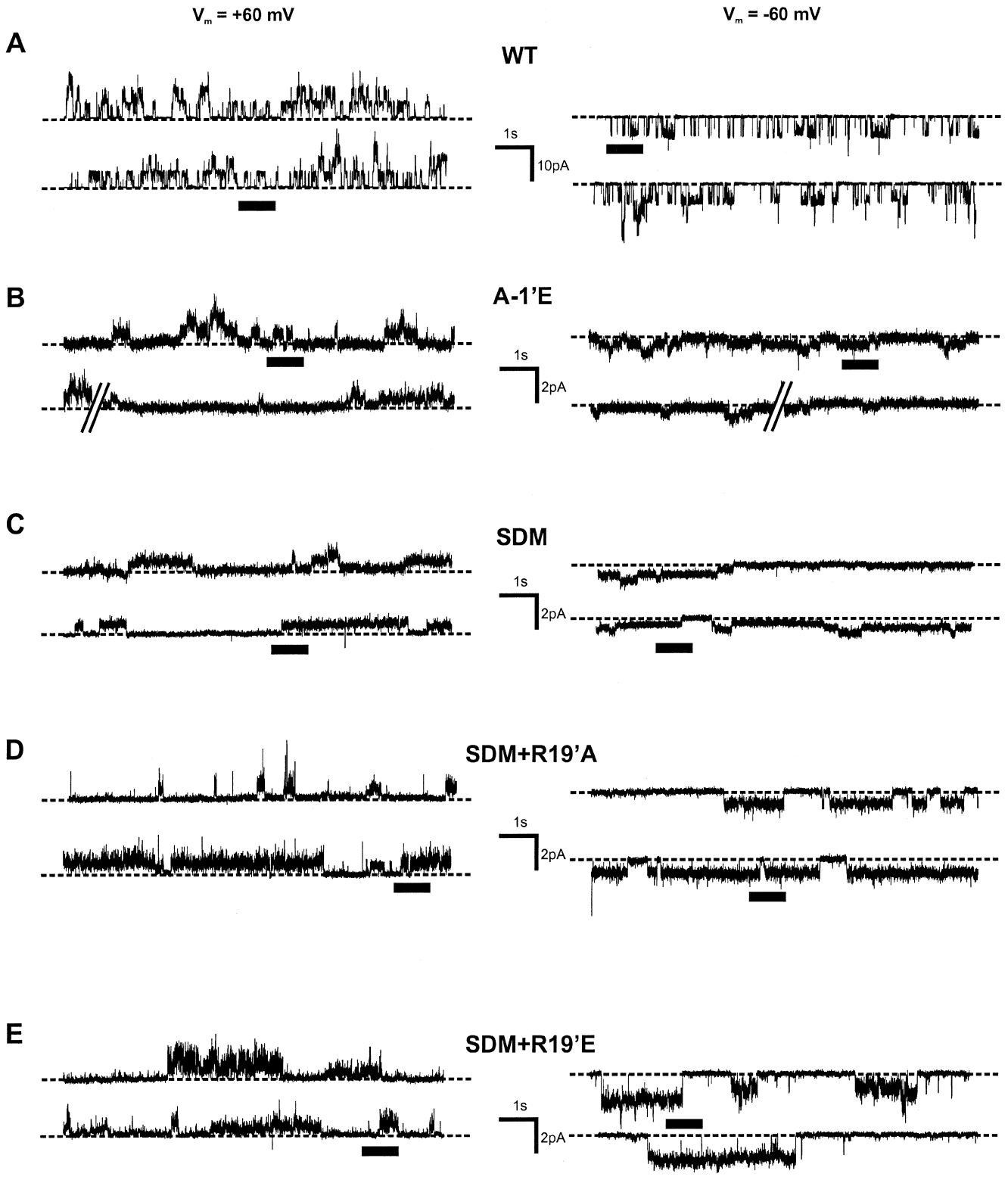

except for the A-1'E mutant GlyR, in which the current recording was interrupted (as indicated by the parallel bars). The dashed lines represent the closed state of the channel. The solid bars below each trace indicate periods of the current recordings that are shown on an expanded scale in Fig. 5. For the WT data, the current recordings come from the same patch as illustrated in Fig. 3. All traces are displayed using the same horizontal (time) scale bar to illustrate the different open times between the WT and the SDM-based GlyRs. Note the different current amplitude scale bars between the WT GlyR and the cation-selective mutant GlyRs. For display, the data were further filtered at a –3 dB of 1 KHz and redigitized at 2.5 KHz.

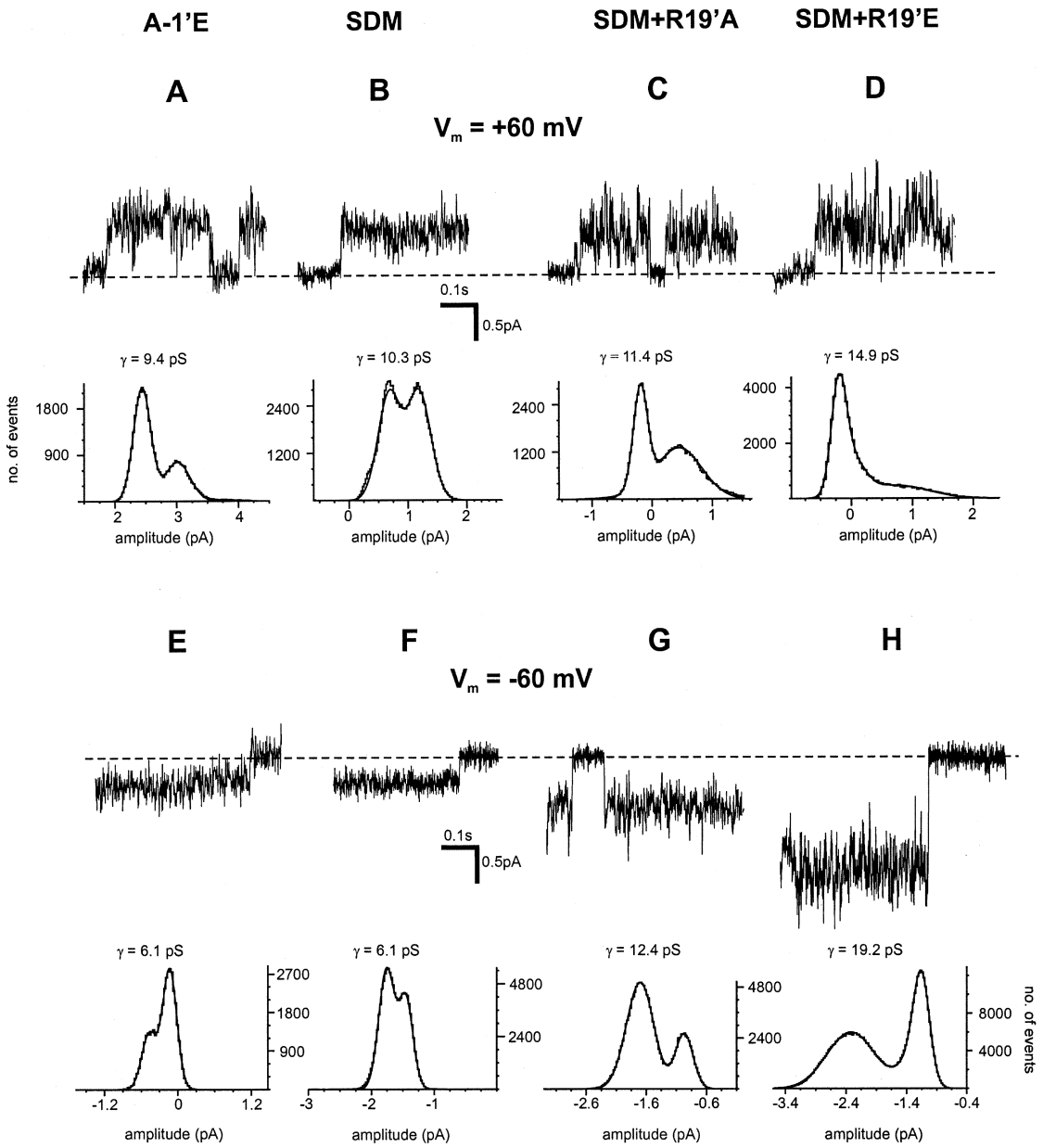

FIGURE 5. Representative single channel currents, and corresponding all-point amplitude histograms, from excised outside-out patches containing cation-selective mutant GlyRs. All currents were recorded in control 145 mM NaCl solutions with divalent cations present (see MATERIALS AND METHODS). The top panels (A–D) show outward currents and corresponding histograms recorded at a membrane potential of 60 mV, whereas the bottom panels (E–H) show inward currents and corresponding histograms recorded from the same patches at a membrane potential of −60 mV. At both potentials the current traces show an expanded ~0.5-s section of the longer recordings shown in Fig. 4 (and indicated by the bars in that figure). The dashed lines represent the closed state of the channels. The all-point amplitude histograms were compiled from longer segments of the same recordings. The overlying curve is the sum of two (A–C and E–H) or three (D) Gaussian distributions fitted to the histograms using a least squares method. The difference between the means of the closed state and the most dominant open state were used to calculate the dominant conductance value for each patch, which is displayed above the histograms. A and E represent the A-1'E GlyR, B and F represent the SDM GlyR, C and G represent the SDM+R19'A GlyR, and D and H represent the SDM+R19'E GlyR.

Effects of Divalent Cations on Conductance of the SDM+R19'A and SDM+R19'E GlyRs

The above experiments were conducted in standard solutions containing 2 mM Ca^{2+} and Mg^{2+} in the external solution and 2 mM Mg^{2+} in the internal solution (2 mM Ca^{2+} was buffered with 5 mM EGTA). Our previous whole cell studies (Keramidas et al., 2002, this issue) demonstrated significant Ca^{2+} permeability in the SDM, SDM+R19'A, and SDM+R19'E GlyRs. This ob-

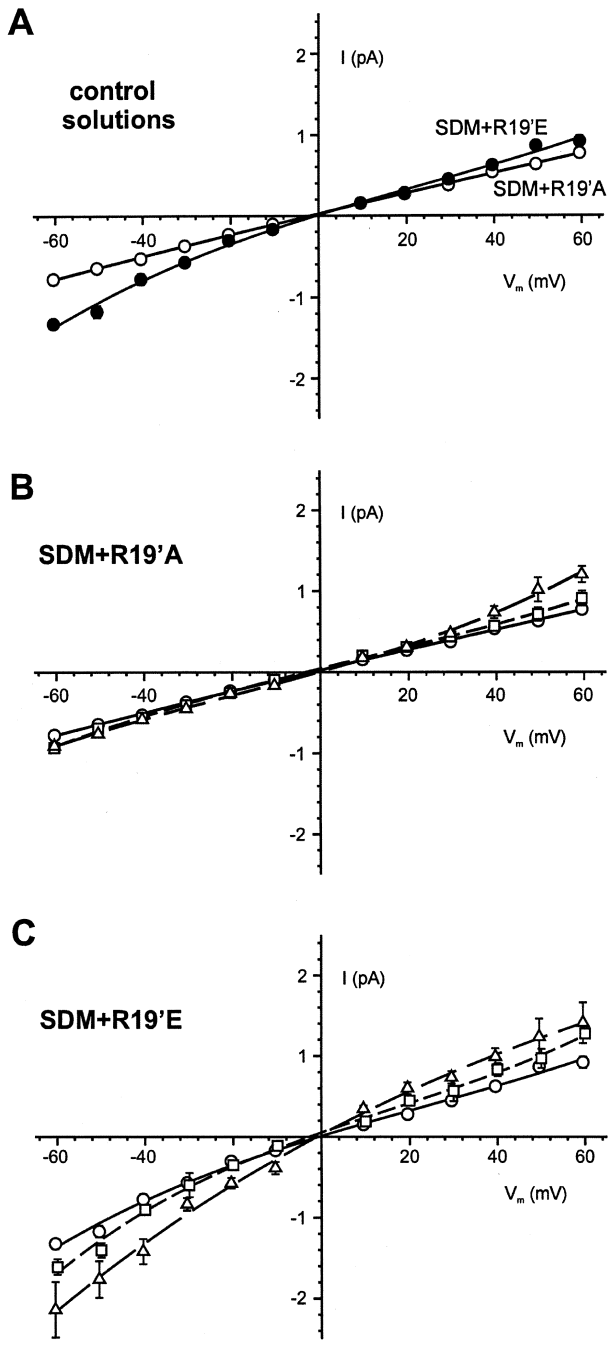

FIGURE 6. Mean I-V curves for the SDM+R19'A and SDM+R19'E GlyRs in the presence and absence of divalent cations. (A) Mean I-V curves for the SDM+R19'A GlyRs (open circles, $n = 5$) and the SDM+R19'E GlyRs (filled circles, $n = 4$) in control solutions (symmetrical 145 mM NaCl with 2 mM Ca^{2+} and 2 mM Mg^{2+} added to both the external and internal solutions and 5 mM EGTA added to the internal solution). (B) Mean I-V curves for the SDM+R19'A GlyRs in control conditions (with divalent ions in both solutions; circles, $n = 5$), when the same five patches were exposed to external solution without Ca^{2+} or Mg^{2+} (squares), and for recordings in which neither the external or internal solution contained Ca^{2+} or Mg^{2+} (triangles, $n = 3$). (C) Mean I-V curves for the SDM+R19'E GlyRs in control conditions (with divalent ions in both solutions; circles, $n = 4$), when the same four patches were exposed to external solution without Ca^{2+} or Mg^{2+} (squares), and for recordings in which neither the external or internal solution contained Ca^{2+} or Mg^{2+} (triangles, $n = 4$). For each patch, current recordings were obtained at all potentials. Error bars, often obscured by the symbol, represent the SEM.

servation, coupled with the well reported inhibitory effects of divalent cations on the nAChR channel monovalent ion conductance (Dani and Eisenman, 1987; Imoto et al., 1988; Kimura et al., 1991), led us to investigate whether the conductance and rectification properties were different in the absence of divalent cations. We investigated the SDM+R19'A and SDM+R19'E GlyRs to assess whether the introduction of a negatively charged residue at the external vestibule position conferred Ca^{2+} sensitivity and a Ca^{2+} binding site(s) on the channel. We used two protocols to examine divalent cation effects: (a) recording channel conductance in standard solutions (with divalent cations) followed by the replacement of the external bath solution with a nominally divalent cation free solution, and (b) measuring channel conductance in the absence of divalent cations in both the external bath and the internal pipette solutions.

The results of these experiments are illustrated in Fig. 6 and the averaged, absolute data summarized in Table III. When divalent cations were removed from the extracellular solution there was no effect on the conductance and rectification properties of the SDM+R19'A GlyRs (Table III; Fig. 6 B). For seven patches held at −50 to −60 mV the relative mean inward conductance in the absence of external divalent cations was 108.1 ± 6.3% of the value obtained in the same patches under the control conditions. For five patches held at 50 or 60 mV the mean relative outward conductance was 109.3 ± 8.8% of the control. The relative R.I. was similarly unaffected (99.1 ± 5.8% of the control, $n = 5$). In contrast, for the SDM+R19'E GlyR, when divalent cations were removed from the external medium there was a significant increase in inward current (Fig. 6 C). In these experiments, the mean relative inward conductance was 113 ± 4% of the control ($n = 6$, $P = 0.02$). The changes in outward conductance were more variable but gave a mean relative conductance of 113 ± 10% of the control ($n = 5$). Hence, the results indicate that in the SDM+R19'E mutant, the 19'E residues create an external ring of negative charge that increases inward conductance and can be shielded by divalent cations in the external solution.

In the second set of experiments, inward and outward conductances were recorded in the absence of divalent cations in both the external and internal solutions. There was an increase in mean inward and outward conductances for the SDM+R19'A and SDM+R19'E GlyRs under these conditions (compare

TABLE III

Effects of Divalent Cations on Conductance and Rectification in the Cation-selective SDM+R19'A and SDM+R19'E GlyRs

	SDM+R19'A GlyR			SDM+R19'E GlyR		
	γ−60mV	γ+60mV	R.I.[a]	γ−60mV	γ+60mV	R.I.[a]
	pS	*pS*	I_{in}/I_{out}	*pS*	*pS*	I_{in}/I_{out}
Control solutions[b]	13.7 ± 0.5 (7)	13.5 ± 0.8 (5)	1.00 ± 0.02 (5)	23.9 ± 1.1 (6)	15.3 ± 1.5 (5)	1.63 ± 0.19 (5)
External Ca^{2+}/Mg^{2+}-free[c]	14.7 ± 0.6 (7)	14.6 ± 1.2 (5)	1.00 ± 0.07 (5)	26.9 ± 1.2[d] (6)	17.5 ± 2.4 (5)	1.67 ± 0.25 (5)
Internal and external Ca^{2+}/Mg^{2+}-free[e]	15.3 ± 1.1 (8)	18.1 ± 1.8[f] (8)	0.87 ± 0.05[f] (8)	31.8 ± 2.9[f] (7)	20.7 ± 3.0 (7)	1.61 ± 0.13 (7)

All data were obtained using excised outside-out patches from 293 cells expressing the cation-selective SDM+R19'A and SDM+R19'E GlyRs. Conductance values were obtained by direct measurements and from Gaussian fits to all-point histograms. The control data were obtained from the same patches that were subsequently exposed to the external divalent cation free conditions, whereas the data for the external and internal divalent ion free conditions were obtained from separate patches. The complete set of control data is shown in Table II. Data presented are mean ± SEM and numbers in parentheses indicate *n*.

[a]As in Table II, the R.I. was derived for each patch as γ−60 mV/γ+60 mV.

[b]The control solution contained approximately symmetrical 145 mM NaCl with 2 mM Ca^{2+} and 2 mM Mg^{2+} in both the external and internal solutions. The internal solution also contained 5 mM EGTA.

[c]The external divalent cation–free solution was the same as the control solution except that Ca^{2+} and Mg^{2+} were omitted.

[d]Significantly different from control data obtained in the same patches (paired *t* test; $P < 0.05$).

[e]The external and internal divalent cation–free solutions were the same as the control solution except that Ca^{2+} and Mg^{2+} were omitted.

[f]Significantly different from the complete set of control data (Table II) obtained in separate patches (unpaired *t* test; $P < 0.05$).

Tables II and III). For the SDM+R19'A GlyR the inward and outward conductances were 15.3 ± 1.1 pS ($n = 8$) and 18.1 ± 1.8 pS ($n = 8$), respectively. At a membrane potential of 60 mV, the outward conductance was significantly greater than the outward conductance recorded in control conditions (where the mean conductance was 13.8 ± 0.6 pS, $n = 12$, Table II, $P = 0.01$). At a membrane potential of −60 mV, the difference in inward conductances measured under control conditions (where the mean conductance was 13.5 ± 0.3 pS, $n = 13$, Table II) and divalent cation free conditions was not significant ($P = 0.06$). The larger increase in outward conductance caused a significant difference in R.I. compared with the control conditions so that the I-V relationship for the SDM+R19'A mutant rectified outwardly (R.I. = 0.87 ± 0.05 in the divalent cation-free conditions and 1.00 ± 0.03 in the control conditions, Table II, $P = 0.03$). For the SDM+R19'E GlyR, the inward and outward conductances were 31.8 ± 2.9 pS ($n = 7$) and 20.7 ± 3.0 pS ($n = 7$), respectively. This represented a significant increase in inward conductance compared with the control conditions (where the mean conductance was 22.2 ± 0.7 pS, $n = 14$, Table II, $P < 0.001$). The increase in mean outward conductance at a membrane potential of 60 mV was not significantly different to the conductance value obtained at 60 mV in the control conditions (where the mean conductance was 16.4 ± 0.8 pS, $n = 13$, Table II, $P = 0.08$) although at 30, 40, and 50 mV the outward conductances were significantly larger than corresponding control values ($P < 0.05$). The mean R.I. in the divalent cation-free conditions (1.61 ± 0.13, $n = 7$) suggested an increase in the extent of inward rectification, but was not significantly different from the value recorded under control conditions (where mean R.I. was 1.40 ± 0.09, $n = 13$, Table II, $P = 0.18$). Hence, when both internal and external divalent cations were removed there were significant increases in outward conductances for both mutant GlyR channels.

We also investigated whether rapid block by divalent cations contributed to the relatively large open channel noise seen in the mutant GlyRs (particularly for the SDM+R19'A and SDM + R19'E GlyRs; Figs. 5 and 6). The increase in the SD of the current upon channel opening was quantified for a random sample of 20 clear single SDM+R19'E GlyR channel openings from 4 different patches in control conditions, and another 20 openings from 4 additional patches in the absence of divalent cations ($V_m = -60$ mV, filtered at −3 dB of 2 kHz). The mean increase in current SD upon channel opening in control conditions was 0.16 ± 0.02 pA, and in divalent cation free conditions was 0.29 ± 0.06 pA. Consequently, rapid divalent cation block of the pore does not contribute to the open channel noise. The higher relative open channel noise in the GlyR mutants may reflect some increase in rapid, small fluctuations in the open pore.

DISCUSSION

The current study investigated the mechanisms of ion permeation in cation-selective GlyRs in an attempt to determine how ion charge selectivity occurs. The accompanying paper (Keramidas et al., 2002, this issue) described a series of mutations flanking the pore-forming M2 domain of the human α1-homomeric GlyR that convert the ion charge selectivity from anion- to cation-selective. In this study, we investigate the permeation characteristics of these cation-selective mutant GlyRs by

recording their single channel conductance and rectification properties and how these properties are affected by divalent cations. In all of the mutants studied (A-1'E, SDM, SDM+R19'A and SDM+R19'E GlyRs), single channel openings were robust and clearly discernible. For the SDM+R19'E GlyR, for example, inward currents ($V_m = -50$ to -60 mV) were large, being ~30 pS in the absence of divalent cations. The inward conductance of α7-homomeric nAChRs in *Xenopus* oocyte cell–attached patches recorded with ~80 mM NaCl pipette solution is ~46 pS (Revah et al., 1991). For other heteromeric nAChR subtypes, inward conductances are similar, ranging from ~30 to 80 pS depending on the recording conditions and subunit composition (e.g., 80 pS for *Torpedo* nAChR, Imoto et al., 1988; and 30 pS in PC12 cells, Neuhaus and Cachelin, 1990; see also Hille, 1992). Thus, the cation conductance of the SDM+R19'E mutant GlyR is comparable to that observed for some nAChRs. This indicates that the mutations induce a clear change in ion charge selectivity, rather than simply reducing relative chloride conductance. The previous WT chloride conductance has been replaced with a significant cation conductance. This implies that there are significant underlying changes in the molecular determinants of permeation in the mutant GlyRs to allow this to occur.

The single channel cation conductance in the mutant GlyRs is lower than the anion conductance in the WT GlyR. This may arise due to intrinsic differences in the physical properties of Na^+ and Cl^- ions (e.g., Cl^- is easier to dehydrate) and how they interact in the different GlyR pores, or due to the influence of other residues, either within or flanking the pore, which have not been mutated (e.g., particularly the R0' and possibly also polar residues within the pore).

Changes in Channel-gating Kinetics

Although the primary aim of this study was an investigation of single channel conductances and their dependence on voltage and divalent cations, we have also provided some preliminary characterization of the different channel gating kinetics seen in the cation-selective GlyRs. The whole-cell currents reveal that all the mutant GlyRs activate more slowly than the WT, and this is particularly true for the three SDM-based GlyRs. The time taken for the current to peak in the SDM-based GlyRs was ~10 times longer (~2 s for the SDM+R19'A and SDM+R19'E GlyRs) than our estimated cell perfusion times (~100–200 ms). The SDM-based mutant GlyRs also showed virtually no current decay in the continued presence of glycine. Fast application of glycine to outside-out patches containing WT α1-GlyRs elicits currents whose decay can be fit well with two exponentials with time constants of 10.6 ± 3.1 ms and 305 ± 212 ms (De Saint Jan et al., 2001). Presumably, our present results describe changes in the slower component of desensitization. The external ring of charge at 19' does not seem to correlate with the extent of current decay, which was similar for all three SDM-based mutant GlyRs. A similar reduced rate of current activation and desensitization is seen in the anion-selective STM 5-HT_3R (Gunthorpe and Lummis, 2001).

The macroscopic current concentration-response curves revealed a decrease in both apparent agonist affinity and in the Hill coefficient for channel activation for the SDM-based mutant GlyRs. For the SDM+R19'A mutant, the EC_{50} was increased ~360-fold as compared with WT GlyRs; for the SDM and SDM+R19'E mutant GlyRs it was increased ~20-fold. Previous studies have identified the R19' residue as being important in channel activation, with a range of mutations of this position to neutral amino acids causing a reduced apparent glycine affinity (Langosch et al., 1994; Rajendra et al., 1995; Lynch et al., 1997). The SDM and SDM+R19'E GlyRs both contain charged amino acids at the R19' position, of opposite polarity, but have a similar concentration-response relationship. This suggests that, in homomeric GlyRs, a ring of either positive or negative charge at the R19' position may be equally compatible with channel activation.

Some of these changes in channel-gating kinetics are also reflected in the microscopic single channel current records. Recombinant α-homomeric GlyRs expressed in *Xenopus* or 293 cells, as well as native spinal GlyRs, typically have mean burst durations at low glycine concentrations of ~5–20 ms (Twyman and Macdonald, 1991; Lewis et al., 1998; Laube et al., 2000). As can be seen in Fig. 4, at low and approximately equipotent glycine concentrations, the SDM-based mutant GlyRs appeared to open for longer periods than those observed for WT GlyRs. This was despite the lower apparent glycine affinity obtained from the concentration-response curves and seems to contrast with the correlation between decreased EC_{50} and increased channel open times for M2 mutated nAChRs (e.g., various mutations to the 9' position; Filatov and White, 1995; Kearney et al., 1996; Kosolapov et al., 2000).

Influence of External Charge on Conductance and Rectification

The voltage dependence of channel conductance of the cation-selective GlyR mutants was investigated to determine the presence and role of charged amino acids, which flank the pore of all LGICs and which are known to have effects on channel conductance in nAChRs and anionic GlyRs (Imoto et al., 1988; Unwin, 1989; Langosch et al., 1994; Rajendra et al., 1995). The A-1'E, the SDM, and also the previously characterized STM GlyRs (Keramidas et al., 2000), in which the na-

tive R19' residue is expected to form an inappropriate external ring of positive charge shows outward rectification with inward cation currents being ~60% of the amplitude of outward currents. This postulated external ring of positive charge would be electrostatically counterproductive for cation permeation in the STM, SDM, and A-1'E mutant GlyRs. When this external ring was neutralized (SDM+R19'A GlyR), inward currents were increased and rectification was lost. When the charge of the external ring was made negative (SDM+R19'E GlyR), inward currents further increased to ~150% of the amplitude of outward currents, resulting in inward rectification. We interpret the observed conductance changes as being due to differences in the rate of cation entry into, and then subsequently through, the pore. A ring of positive charges would be expected to increase the barrier for cation permeation into the pore and reduce the local cation concentration in the extracellular pore vestibule, whereas a negative ring of charges would have the opposite effect (see below; see also Dani, 1986; Green and Andersen, 1991; Hille, 1992). The fact that the changes in the polarity of fixed vestibule charges had the expected effects on conductance also suggests common permeation mechanisms between cation-selective mutated GlyRs and other members of the LGIC superfamily. This supports the suggestion that the selectivity-converting mutations have only had local conformational effects and have not disrupted the gross structure of the entire pore.

The lack of rectification when the external ring is neutralized suggests a symmetrical barrier for cation permeation in both directions through the SDM+R19'A GlyR. We propose that the GlyR selectivity mutations change the dominating charge at the intermediate ring position and that the conductance characteristics are dominated by the side chain charge at the intermediate ring, as also suggested for nAChRs (Imoto et al., 1988; Forster and Bertrand, 1995). The linear current-voltage relationship for the SDM+R19'A GlyR therefore suggests that the intermediate ring affects inward and outward conductances equally. Furthermore, this suggests that, in the mutant GlyRs at least, the ring of negative charges at the cytoplasmic pore vestibule (D-5′; Fig. 1) does not contribute significantly to permeation. This contrasts with the nAChRs, in which the cytoplasmic ring of negative charges at the equivalent position does contribute to cation conductance, and particularly to the outwardly directed cation flux, although not to the same degree as the intermediate ring (Imoto et al., 1988). Perhaps not surprisingly, the charge on the cytoplasmic ring does not seem to contribute markedly to permeation in the cation-selective mutant GlyRs, as a ring of exposed negative charges would be counterproductive to achieving robust anion transport through native GlyRs.

Effects of Divalent Cations on Conductance and Rectification

Fixed negative charges from acidic amino acids in or around the pore of many cation-selective channels are the sites of interactions with divalent and polyvalent cations, as, for example, in inwardly rectifying K^+ channels (for review see Nichols and Lopatin, 1997), cyclic-nucleotide–gated channels (Root and MacKinnon, 1993), and voltage-dependent Ca^{2+} and Na^+ channels (Heinemann et al., 1992; Yang et al., 1993). Similarly, in nAChRs, the inhibitory effects of Mg^{2+} on monovalent cation conductance are due to interactions with the internal and external rings of charges (Imoto et al., 1988; Forster and Bertrand, 1995). Ca^{2+} and other divalent cations also inhibit the conductance of monovalent ions through nAChRs (Imoto et al., 1986; Dani and Eisenman 1987; Neuhaus and Cachelin, 1990; Kimura et al., 1991), although the exact molecular determinants of this effect are unknown. For both Ca^{2+} and Mg^{2+}, however, the inhibition is sensitive to the side from which the divalent ions are applied, with, for example, typically greater inhibition of inward currents when the ions are added to the extracellular side, consistent with an action on the external rings of charge flanking the channel pore. Hence, we investigated the effects of divalent cations on conductance in order to explore the presence of negative rings of charge flanking the pores of the cation-selective mutant GlyRs. For WT α1 GlyRs expressed in 293 cells, Ca^{2+} has no direct effect on the single channel conductance (Fucile et al., 2000). In the current study, nominally divalent cation-free external solutions increased the magnitude of inward currents through SDM+R19'E GlyRs, but not through SDM+R19'A GlyRs. This confirms that the external ring of negative charge in the SDM+R19'E GlyR creates an interaction site for external divalent cations. Furthermore, as was also seen with the difference between the SDM+R19'A and SDM+R19'E GlyRs, only the inward conductance was increased, suggesting that the negative charge only reduces the barrier for external cation entry into the pore.

We also investigated the effects of removing both extracellular and intracellular divalent cations. It should be noted that, since the Ca^{2+} concentration in the pipette solution was buffered by EGTA, removal of divalent cations from the pipette solution effectively equated to removal of Mg^{2+}. Under these conditions, inward currents through SDM+R19'E GlyRs were further increased and there was a marginal increase in inward currents through the SDM+R19'A GlyRs. Both of the mutant GlyR channels showed a clear and significant increase in outward currents under these conditions. Thus, the pattern of changes observed was very similar to the effects of Mg^{2+} ions shielding of the intermediate ring in the nAChR (Imoto et al., 1988). We interpret these results as evidence for a ring of negative

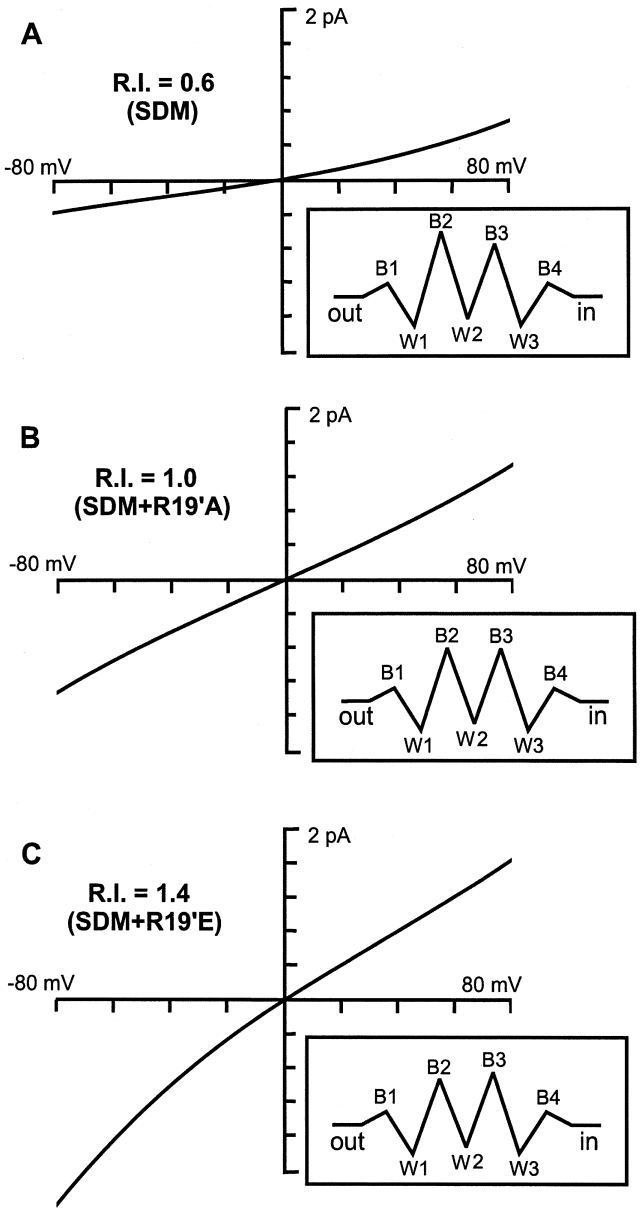

FIGURE 7. A set of schematic I-V curves generated from a 4-barrier, 3-site rate theory model of ion permeation (modified from Hille, 1975), intended to show how variations in one rate theory parameter can semiquantitatively simulate the changes in rectification observed at the single channel level for the cation-permeant mutant GlyR channels, when the charge in the external 19' position is changed from a positive arginine (SDM) to a neutral alanine (SDM+R19'A) or to a negative glutamate (SDM+R19'E). The (potential independent) barrier heights are indicated as B1, B2, B3, and B4, and the well depths for the sites as W1, W2, and W3. The potential independent energy profile is shown schematically in the inset boxes beside each plot. It should be noted that the only parameter being changed between the I-V curves is the main external barrier height, B2. The highest barrier height simulates the case for the positively charged arginine present (9 RT), the symmetrical case, the neutral alanine (7.5 RT, the same as B3), and the lowest barrier height, the negatively-charged glutamate (6.5 RT). The R.I. shown has been calculated as $I_{(-60\ mV)}/I_{(60\ mV)}$, and is close to the experimental values given in Table II for the appropriate mutant GlyR and shown in parentheses with each plot. It should also be noted that the model only allows one ion to be present in the pore at any one time. In addition, the model requires W2 to be less deep than W1 or W3 in order to get reasonably shaped I-V curves. The slightly greater decrease in absolute conductance for the SDM-simulated case (Fig. 7 A), compared with the SDM+R19'A (Fig. 7 B) and the SDM+R19'E (Fig. 7 C), may also reflect the above model limitation.

charges at the internal end of the pore and suggest that this arises due to the −1'E acidic side chains. The magnitude of the effect of Mg^{2+} on conductance was not, however, as marked as in nAChRs (Imoto et al., 1988). Perhaps the preponderance of positively charged residues in the internal M3-M4 loop of the GlyR, which have been speculated to line an intracellular vestibule region and contribute to ionic selectivity in the nAChR (Miyazawa et al., 1999), electrostatically reduce the access of Mg^{2+} to the constricted region.

Modeling of Ion Permeation in the SDM-based Cation-selective GlyRs

The four barrier, three site rate theory model of ion permeation of Hille (1975), modified for only one permeant ion species and with most of the voltage drop (96%) occurring across the two central barriers, was used to see whether modulation of a single barrier height (or well depth) could simulate the rectification pattern seen for the SDM-based mutant GlyRs when the charge on the external ring (R19') was changed from positive to neutral and then to negative. It seems reasonable to assume that these changes would affect either the main external barrier height (B2), or well depth (W1), or both. As can be seen from Fig. 7, changes in barrier height alone could simulate the changes in rectification observed at the single channel level for the cation-permeant mutant GlyR channels. Changes in well depth did not control rectification in the same sort of way. This latter observation may reflect the shortcomings of the model, which, for ease of mathematical manipulation, assumes that only one ion can be in the channel at any one time. Nevertheless, in the absence of more precise modeling, the above rate theory model does show that our interpretation of the effects of charge modification is very reasonable.

Mechanisms Underlying Charge Selectivity Conversion

Energy barriers arising due to changes in dielectric constant as an ion attempts to permeate through a membrane channel can be overcome by the presence of polar groups or fixed charges in or around the channel wall (e.g., Dani, 1986; Hille, 1992; Hoyles et al., 1996). In the mutant GlyRs, we suggest that the cation flux observed is achieved as a result of the polarity of these fixed charges in the intermediate charged ring, being changed from positive to negative. We postulate that the critical change

is the glutamate residue introduced into the −1' position, which provides the negative electrostatic environment and a relative energy well for cation permeation. This hypothesis is strongly supported by the divalent cation effects. As also observed in nAChRs (Imoto et al., 1988; Kienker et al., 1994; Forster and Bertrand, 1995), Mg^{2+} applied from the intracellular side of the membrane shielded the intermediate ring of charge, which decreased both inward and, particularly, outward conductances. Extracellular divalent ions only affected the inward conductance, and only when a fixed negative charge was introduced into the external vestibule. The conductance values and pattern of rectification was also consistent with the presence of a ring of negative charges at the intermediate position. Due to the pore tapering to a constriction in this region (by analogy with other LGICs; Lester, 1992; Wilson and Karlin, 1998), the effectiveness of any point charge will be enhanced (Dani, 1986; Hoyles et al., 1996). Hence, only a slight change in the net electric field in this region could have marked effects on permeation. The proline deletion at −2' (SDM GlyR) does not seem to markedly change the barrier heights or electric potential in the pore, as judged by an absence of changes in rectification and conductance compared with the A-1'E mutant GlyR, but does accentuate relative cation permeability, perhaps by a subtle change in the pore dimensions (Keramidas et al., 2002, this issue). The changes in pore diameter seen in the different cation-selective GlyRs did not show any correlation with the changes in single channel conductance. Furthermore, it does not seem that the influence of the external ring on conductance is mediated through indirect changes in minimum pore diameter. This supports our inference that the effects of this external charge on conductance are due to electrostatic effects, rather than due to changes in minimum pore diameter. Whether the electrostatic effects of this 19' external charge behave like a simple point charge, or acts in a somewhat more complex manner, as suggested for the nAChR charge manipulations (Kienker et al., 1994), is not clear. The effects of the point mutations in the GlyR were quite asymmetrical, enabling the conductance and rectification pattern to be successfully modeled with changes only in the main external barrier height (see above). This differed from equivalent nAChR data (Kienker et al., 1994), indicating that the electrostatic effects of the 19' point mutations in the homomeric α1-GlyRs may be different and more straightforward to interpret than for those in heteromeric nAChRs.

Conclusion

In this study, we have investigated the conductance and rectification properties of a series of cation-selective mutant GlyRs using single channel recordings. All of the cation-selective mutants showed reasonably large conductances, ranging from ~6 to 22 pS at −60 mV, or even higher in the absence of divalent cations. The differences in the single channel rectification patterns amongst the mutant GlyRs depended on the presence and polarity of a ring of charged residues in the 19' position at the external pore vestibule, as did the inhibition of inward currents by externally applied divalent cations. The inhibition of outward currents by internally applied divalent cations suggested a ring of negatively charged residues located at the internal end of the channel pore. Hence, these studies support the hypothesis that the charge selectivity mutations only cause local changes in the selectivity filter region of the channel pore and that these local changes involve the introduced glutamate at position −1' becoming exposed so that it now electrostatically dominates over the adjacent arginine (R0'). We propose that ion charge selectivity in LGICs is primarily achieved by an appropriate electrostatic environment at the selectivity filter of the pore. The data also show that channel conductance and rectification is strongly influenced by the electrostatic environment at the extracellular mouth of the ion channel, and that this seems to be a general feature throughout the LGIC family.

We thank Dr. Kerrie Pierce for constructing the GlyR mutant cDNAs; Irene Michas and Anna Scimone for maintenance of the 293 cells; and Dr. Trevor Lewis for comments on the manuscript.

This study was funded by the National Health and Medical Research Council of Australia (NH&MRC Project Grant 993584, NH&MRC Block Grant 993050) and a 2002 University Research Support Program Grant (URSP).

Submitted: 27 December 2001
Revised: 22 March 2002
Accepted: 22 March 2002

REFERENCES

Barry, P.H. 1994. *JPCalc*, a software package for calculating liquid junction potential corrections in patch-clamp, intracellular, epithelial and bilayer measurements and for correcting junction potential measurements. *J. Neurosci. Methods.* 51:107–116.

Barry, P.H., and K. Fatima-Shad. 1995. Ion permeation through ligand-gated ion channels. *Today's Life Sci.* 7:32–37.

Changeux, J.P. 1993. Chemical signalling in the brain. *Sci. Am.* 269: 58–62.

Chen, C., and H. Okayama. 1987. High efficiency expression of mammalian cells by plasmid DNA. *Mol. Cell. Biol.* 7:2745–2751.

Corringer, P.J., S. Bertrand, J.L. Galzi, A. Devillers-Thiéry, J.P. Changeux, and D. Bertrand. 1999. Mutational analysis of the charge selectivity filter of the α7 nicotinic acetylcholine receptor. *Neuron.* 22:831–843.

Couturier, S., D. Bertrand, J.M. Matte, M.C. Hernandez, S. Bertrand, N. Millar, S. Valera, T. Barkas, and M. Ballivet. 1990. A neuronal nicotinic acetylcholine receptor subunit (α 7) is developmentally regulated and forms a homo-oligomeric channel blocked by α-BTX. *Neuron.* 5:847–856.

Dani, J.A. 1986. Ion-channel entrances influence permeation. *Biophys. J.* 49:607–618.

Dani, J.A., and G. Eisenman. 1987. Monovalent and divalent cation

permeation in acetylcholine receptor channels. Ion transport related to structure. *J. Gen. Physiol.* 89:959–983.

De Saint Jan, D., B. David-Watine, H. Korn, and P. Bregestovski. 2001. Activation of human α1 and α2 homomeric glycine receptors by taurine and GABA. *J. Physiol.* 535:741–755.

Filatov, G.N., and M.M. White. 1995. The role of conserved leucines in the M2 domain of the acetylcholine receptor in channel gating. *Mol. Pharmacol.* 48:379–384.

Forster, I., and D. Bertrand. 1995. Inward rectification of neuronal nicotinic acetylcholine receptors investigated by using the homomeric alpha 7 receptor. *Proc. R. Soc. Lond. B Biol. Sci.* 260:139–148.

Fucile, S., D. De Saint Jan, L.P. de Carvalho, and P. Bregestovski. 2000. Fast potentiation of glycine receptor channels of intracellular calcium in neurons and transfected cells. *Neuron.* 28:571–583.

Galzi, J.L., A. Devillers-Thiéry, N. Hussey, S. Bertrand, J.P. Changeux, and D. Bertrand. 1992. Mutations in the channel domain of a neuronal nicotinic receptor convert ion selectivity from cationic to anionic. *Nature.* 359:500–505.

Green, W.N., and O.S. Andersen. 1991. Surface charges and ion channel function. *Annu. Rev. Physiol.* 53:341–359.

Grenningloh, G., A. Rienitz, B. Schmitt, C. Methfessel, M. Zensen, K. Beyreuther, E.D. Gundelfinger, and H. Betz. 1987. The strychnine-binding subunit of the glycine receptor shows homology with nicotinic acetylcholine receptors. *Nature.* 328:215–220.

Gunthorpe, M.J., and S.C. Lummis. 2001. Conversion of the ion selectivity of the 5-HT(3a) receptor from cationic to anionic reveals a conserved feature of the ligand-gated ion channel superfamily. *J. Biol. Chem.* 276:10977–10983.

Heinemann, S.H., H. Terlau, W. Stuhmer, K. Imoto, and S. Numa. 1992. Calcium channel characteristics conferred on the sodium channel by single mutations. *Nature.* 356:441–443.

Hille, B. 1975. Ionic selectivity, saturation, and block in sodium channels. A four-barrier model. *J. Gen. Physiol.* 66:535–560.

Hille, B. 1992. Ionic Channels of Excitable Membranes. 2nd ed. Sinauer Associates, Inc., Sunderland, MA. 607 pp.

Hoyles, M., S. Kuyucak, and S.H. Chung. 1996. Energy barrier presented to ions by the vestibule of the biological membrane channel. *Biophys. J.* 70:1628–1642.

Imoto, K. 1993. Ion channels: molecular basis of ion selectivity. *FEBS Lett.* 325:100–103.

Imoto, K., C. Busch, B. Sakmann, M. Mishina, T. Konno, J. Nakai, H. Bujo, Y. Mori, K. Fukuda, and S. Numa. 1988. Rings of negatively charged amino acids determine the acetylcholine receptor channel conductance. *Nature.* 335:645–648.

Imoto, K., C. Methfessel, B. Sakmann, M. Mishina, Y. Mori, T. Konno, K. Fukuda, M. Kurasaki, H. Bujo, Y. Fujita, and S. Numa. 1986. Location of a δ-subunit region determining ion transport through the acetylcholine receptor channel. *Nature.* 324:670–674.

Karlin, A., and M.H. Akabas. 1995. Towards a structural basis for the function of nicotinic ecetylcholine receptors and their cousins. *Neuron.* 15:1231–1244.

Kearney, P.C., H. Zhang, W. Zhong, D.A. Dougherty, and H.A. Lester. 1996. Determinants of nicotinic receptor gating in natural and unnatural side chain structures at the M2 9' position. *Neuron.* 17:1221–1229.

Keramidas, A., A.J. Moorhouse, C.R. French, P.R. Schofield, and P.H. Barry. 2000. M2 pore mutations convert the glycine receptor channel from being anion- to cation-selective. *Biophys. J.* 78:247–259.

Keramidas, A., A.J. Moorhouse, K.D. Pierce, P.R. Schofield, and P.H. Barry. 2002. Cation selective mutations in the M2 domain of the inhibitory glycine receptor channel reveal determinants of ion-charge selectivity. *J. Gen. Physiol.* 119:393–410.

Kienker, P., G. Tomaselli, M. Jurman, and G. Yellen. 1994. Conductance mutations of the nicotinic acetylcholine receptor do not act by a simple electrostatic mechanism. *Biophys. J.* 66:325–334.

Kimura, I., H. Nojima, and M. Kimura. 1991. External Ca^{2+} dependence of acetylcholine- and succinylcholine-induced changes in channel conductance, open time and frequency at endplates of single muscle cells of adult mice. *Neuropharmacology.* 30:1211–1217.

Kosolapov, A.V., G.N. Filatov, and M.M. White. 2000. Acetylcholine receptor gating is influenced by the polarity of amino acids at position 9' in the M2 domain. *J. Membr. Biol.* 174:191–197.

Langosch, D., B. Laube, N. Rundstrom, V. Schmieden, J. Bormann, and H. Betz. 1994. Decreased agonist affinity and chloride conductance of mutant glycine receptors associated with human hereditary hyperekplexia. *EMBO J.* 13:4223–4228.

Laube, B., J. Kuhse, and H. Betz. 2000. Kinetic and mutational analysis of Zn^{2+} modulation of recombinant human inhibitory glycine receptors. *J. Physiol.* 522:215–230.

Lester, H.J. 1992. The permeation pathway of neurotransmitter-gated ion channels. *Annu. Rev. Biophys. Biomol. Struct.* 21:267–292.

Lewis, T.M., L.G. Sivilotti, D. Colquhoun, R.M. Gardiner, R. Schoepfer, and M. Rees. 1998. Properties of human glycine receptors containing the hyperekplexia mutation α1(K276E), expressed in *Xenopus* oocytes. *J. Physiol.* 507:25–40.

Lynch, J.W., S. Rajendra, K.D. Pierce, C.A. Handford, P.H. Barry, and P.R. Schofield. 1997. Identification of intracellular and extracellular domains mediating signal transduction in the inhibitory glycine receptor chloride channel. *EMBO J.* 16:110–120.

Miyazawa, A., Y. Fujiyoshi, M. Stowell, and N. Unwin. 1999. Nicotinic acetylcholine receptor at 4.6 Å resolution: transverse tunnels in the channel wall. *J. Mol. Biol.* 288:765–786.

Moorhouse, A.J., P. Jacques, P.H. Barry, and P.R. Schofield. 1999. The startle disease mutation Q266H, in the second transmembrane domain of the human glycine receptor, impairs gating. *Mol. Pharmacol.* 55:386–395.

Neuhaus, R., and A.B. Cachelin. 1990. Changes in the conductance of the neuronal nicotinic acetylcholine receptor channel induced by magnesium. *Proc. R. Soc. Lond. B. Biol. Sci.* 241:78–84.

Nichols, C.G., and A.N. Lopatin. 1997. Inward rectifier potassium channels. *Annu. Rev. Physiol.* 59:171–191.

Rajendra, S., J.W. Lynch, K.D. Pierce, C.R. French, P.H. Barry, and P.R. Schofield. 1995. Mutation of an arginine residue in the human glycine receptor transforms β-alanine and taurine from agonists to competitive antagonists. *Neuron.* 14:169–175.

Revah, F., D. Bertrand, J.L. Galzi, A. Devillers-Thiery, C. Mulle, N. Hussy, S. Bertrand, M. Ballivet, and J.P. Changeux. 1991. Mutations in the channel domain alter desensitization of a neuronal nicotinic receptor. *Nature.* 353:846–849.

Root, M.J., and R. MacKinnon. 1993. Identification of an external divalent cation-binding site in the pore of a cGMP-activated channel. *Neuron.* 11:459–466.

Twyman, R.E., and R.L. Macdonald. 1991. Kinetic properties of the glycine receptor main- and sub-conductance states of mouse spinal cord neurones in culture. *J. Physiol.* 435:303–331.

Unwin, N. 1989. The structure of ion channels in membranes of excitable cells. *Neuron.* 3:665–676.

Unwin, N. 1993. Neurotransmitter action: opening of ligand-gated ion channels. *Cell.* 72:31–41.

Wilson, G.G., and A. Karlin. 1998. The location of the gate in the acetylcholine receptor channel. *Neuron.* 20:1269–1281.

Yang, J., P.T. Ellinor, W.A. Sather, J.F. Zhang, and R.W. Tsien. 1993. Molecular determinants of Ca^{2+} selectivity and ion permeation in L-type Ca^{2+} channels. *Nature.* 366:158–161.